

Numerical Simulation Study Using a Climate Model Including a Sophisticated Land Surface Model

Kazuo MABUCHI¹, Yasuo SATO¹ and Hideji KIDA²

¹*Meteorological Research Institute, Ibaraki 305-0052, Japan*

²*Kyoto University, Kyoto 606-8502, Japan*

INTRODUCTION

Numerical simulations were used to investigate the mechanisms of the physical and biological interactions between the terrestrial ecosystems and climate on a regional scale. Also, a study was conducted on how the regional interactions influence seasonal and interannual variations of the regional atmospheric carbon dioxide concentrations. The numerical simulation was performed using a physical regional climate model, including a sophisticated biological land surface model. The experimental area includes the Japanese Islands and surrounding area. The regional climate model can estimate the nonlinear physical and biological interactions between terrestrial ecosystems and the atmosphere using a short time step (only several minutes), and a fine grid scale (about 30 km).

MODEL DESCRIPTION

The regional climate model used in the present study is the Japan Spectral Model (JSM) including the Biosphere–Atmosphere Interaction Model (BAIM) (Mabuchi *et al.*, 1997, 2000, 2001). Hereafter, this regional climate model is referred to as the JSM-BAIM.

The model employs sigma coordinates with 23 levels in the vertical. The model has a regular 129×129 square transform grid on a polar stereographic projection plane, which translates to a horizontal resolution of 30 km at 60°N. The basic equations adopted in the model are the primitive equations, and the prognostic atmospheric variables are temperature, specific humidity, the zonal and meridional components of the wind, and surface pressure. In the JSM-BAIM, the concentration of atmospheric carbon dioxide was added to the prognostic variables. The model includes radiation processes. The short-wave and the long-wave radiation processes are calculated. Precipitation is predicted by three processes; that is, large-scale condensation, moist convective adjustment, and evaporation of raindrops. Vertical diffusion is calculated by a turbulent closure model.

Land surface processes are calculated within the BAIM. The BAIM has two vegetation layers and three soil layers, and predicts the temperature and stored

moisture for each layer. In the presence of snow cover, the snow layer is divided into a maximum of three layers, with the temperature and amount of snow and water stored in each layer being predicted. Photosynthesis processes for C_3 and C_4 plants are adopted in the model. Not only the energy fluxes, but also the carbon dioxide flux between terrestrial ecosystems and the atmosphere are estimated by the BAIM. The model can also predict the ground accumulation and melting of snow, and the freezing and melting of water in the soil. The type of vegetation at each model grid point is specified, and land surface processes at each grid point are calculated by the BAIM.

EXPERIMENTAL DESIGN

Two boundary coupling methods are simultaneously used during the time integrations. One is the time-dependent lateral boundary coupling (LBC) as proposed by Tatsumi (1986), the other is the spectral boundary coupling (SBC) by Kida *et al.* (1991). In the LBC method, the lateral boundary conditions, determined by linear interpolation from boundary data, are prescribed at each time step of the integration. In the SBC method, the long-wave components of the boundary data, and the short-wave components of the calculated results of the nested regional model, are joined in a wave-number space at a selected periodic time. The joined field then becomes the new initial field as the time integration continues.

Meteorological boundary condition data for the JSM-BAIM were created from the global objective analysis data. Using the 12-hour interval analysis data (00 and 12 UTC of each day), the JSM-BAIM grid point data were interpolated, and then used for the initial conditions, lateral boundary conditions, and spectral boundary conditions of the model. The boundary conditions for the carbon dioxide concentrations were taken from the 8 km-tropopause data observed over Japan (Nakazawa *et al.*, 1993). From the observed data, 12 hourly interval data

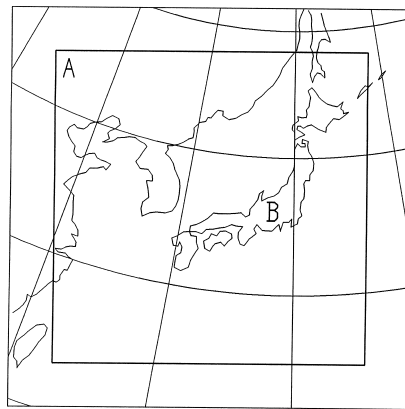


Fig. 1. Domain of JSM-BAIM and areas examined, Areas A and B.

were made. For the SBC of this experiment, the spectral boundary wave-number was set to 3, and applied to the temperature, and the zonal and meridional wind components fields at each level above the 0.53 sigma level.

There are 15 types of vegetation employed in the JSM-BAIM domain. The sea surface temperature data, sea ice data, and the carbon dioxide fluxes between the sea surface and atmosphere for the JSM-BAIM sea-area grid points were prescribed through estimated values taken from the observed data. For further details, the reader should refer to Mabuchi *et al.* (2000).

To estimate the initial values of soil wetness, including the ice content in the soil and soil temperature, ten time integrations over a 1-year period from 12 UTC 31 July 1985, to 12 UTC 31 July 1986, were carried out. Using the soil values obtained by the ten yearly pre-runs as the initial conditions, the experimental time integrations were started at 12 UTC 31 July 1985 and continued until 12 UTC 31 December 1991, for a total of 6 years and 5 months.

RESULTS

Experimental results for the 6-year period from 1 January 1986 to 31 December 1991 were examined. Figure 1 shows the domain of the JSM-BAIM and areas examined. Two areas were chosen for the examination. Area A covers

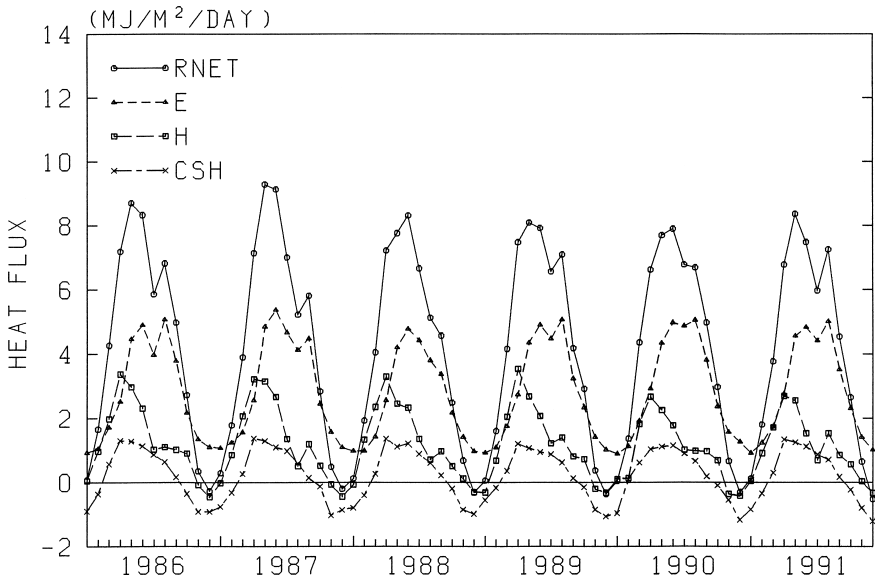


Fig. 2. Temporal distributions of the heat fluxes ($\text{MJ m}^{-2}\text{day}^{-1}$) calculated by the model. The values are monthly means averaged over the land area within Area A. Distributions are shown for RNET, the net radiation flux (downward flux is positive), E, the latent heat flux (upward flux is positive), H, the sensible heat flux (upward flux is positive), and CSH, the residual of the heat balance.

the entire domain of the JSM-BAIM, except for the model's lateral boundary areas. Area B represents only the Japanese Islands.

Comparisons of the model results with the analysis data were performed. Differences in the geopotential height field, temperature field, and wind field at the 850 hPa level were mainly attributed to differences in resolution between the regional climate model field and the analysis data field. Differences at the 500 hPa level were relatively small. As a result of using the SBC method, there were no large-scale phase differences between the model results and the analysis data, both at the 850 hPa and 500 hPa levels. Comparisons of the model results with the data observed by the Automated Meteorological Data Acquisition System (AMeDAS) were performed for the precipitation, surface air temperature, and the radiation, over land in the area of the Japanese Islands. The model reproduced the seasonal and regional changes and interannual variations in precipitation, temperature, and radiation.

Figure 2 shows the monthly means of the area mean heat budgets of land areas within Area A as estimated by the model. Although there are no observed data with which the model results can be directly compared, the seasonal cycles and the proportion of each flux element to the net radiation flux are appropriate for heat flux values of vegetated land surface areas. The net radiation fluxes in 1986 and in 1987 are somewhat stronger than those in other years.

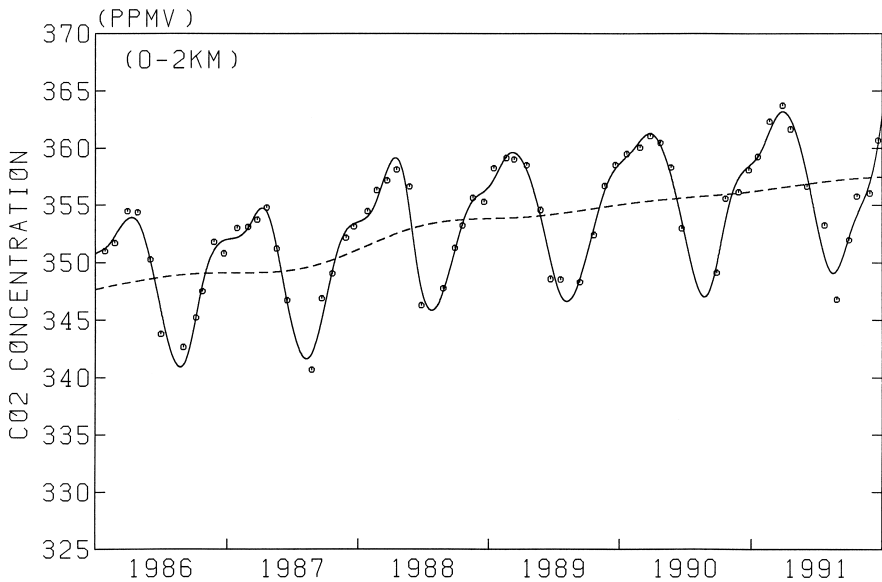


Fig. 3. Temporal distribution of the carbon dioxide concentrations (ppmv) for the 0–2 km layer observed over Japan. Open circles are the observed data (Nakazawa *et al.*, 1993; Nakazawa, personal communication). Solid line is best fit curve of the observed data, and broken line is the long-term trend.

Figure 3 shows the carbon dioxide concentrations (CDCs) for the 0–2 km layer as observed over Japan. The seasonal cycles of the CDCs are very clear. These seasonal cycles are mainly produced by seasonally-dependent biosphere activity. Another characteristic of the CDC appears in the long-term trends. The long-term trend exhibits a near stepwise increase in the CDC from 1987 to 1988. This stepwise increase in the long-term trend of the CDC is not clearly seen in the upper troposphere (Nakazawa *et al.*, 1993).

Figure 4 shows the averaged values of the CDC at the 900 and 850 hPa levels calculated by the model. Although the amplitudes of the seasonal cycles are small and the patterns differ compared with those actually observed (Fig. 3) because the boundary condition values of the CDC prescribed for the model did not have seasonal cycles, the characteristic phenomenon of the stepwise increase in the long-term trend of the CDCs from 1987 to 1988 is reproduced.

Figure 5 shows the carbon dioxide fluxes between the land surface and atmosphere calculated by the model. The values of AAT during 1986 and 1987 are apparently stronger than those in 1988 and the following years. Consequently, the values of NET during 1986 and 1987 are also stronger than those in the following years. The large values of NET in 1986 and 1987 relate to the conspicuously low values of the CDC in the lower troposphere during the growing seasons of 1986 and 1987.

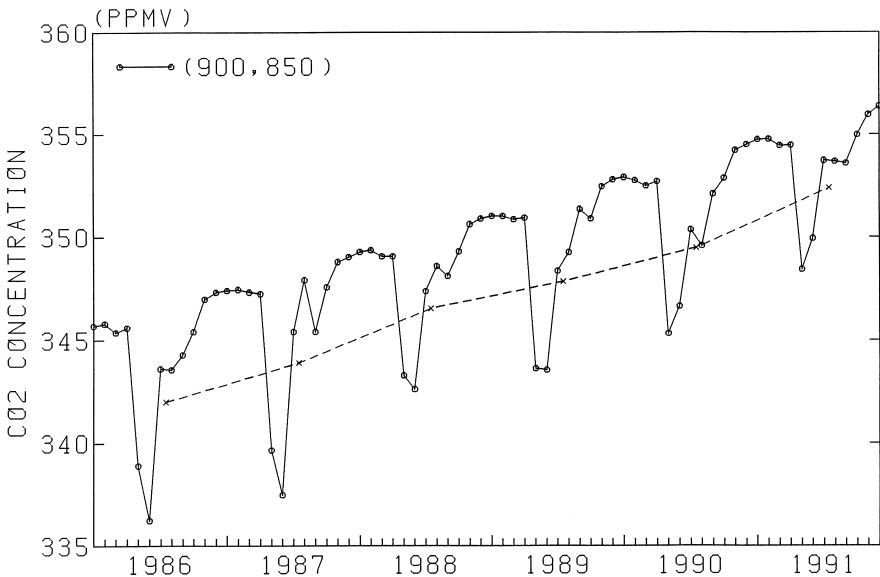


Fig. 4. Temporal distribution of the carbon dioxide concentrations (ppmv) calculated by the model. Open circles are the mean values of the monthly 900 and 850 hPa values in Area B. The X symbols are 6-month mean values (May through October) for each year.

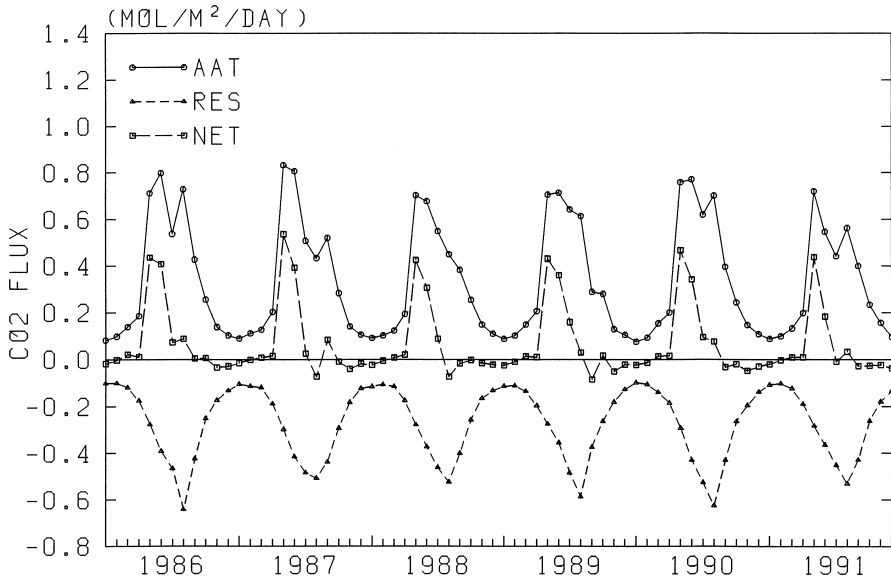


Fig. 5. Temporal distributions of the carbon dioxide fluxes ($\text{mol m}^{-2}\text{day}^{-1}$) between the land surface and atmosphere calculated by the model. The values are monthly means averaged over Area B. The values of AAT are the total carbon dioxide assimilation flux (downward flux is positive), RES is the total respiration flux (upward flux is negative), and NET is the net carbon dioxide flux (downward flux is positive).

The values of the carbon dioxide absorption flux are influenced by the stomatal resistance of vegetation. Table 1 lists the interannual variations of the principal elements that influence the stomatal resistance of vegetation with those of other physical quantities. Among the principal elements, the values of downward short-wave radiation indicate high values of positive correlation with the NET values. This fact suggests that the values of NET should be large during the years when the short-wave radiation (namely the photosynthetically active radiation) was strong, and vice versa. The value of the correlation coefficient between NET and the soil water content has a negative value. The correlation between NET and the surface relative humidity also indicates a negative value. These facts suggest that the interannual variations in NET during the present experimental period were not influenced by the soil water content and humidity around the vegetation leaves. The correlation coefficient between the NET and precipitation indicates a negative value. The interannual patterns of precipitation correspond with those of the soil water content and relative humidity. Therefore, it is inferred that the interannual variations in the soil water content and the relative humidity are due to the interannual variations in precipitation. The interannual patterns of precipitation are qualitatively opposite those of the downward short-wave radiation.

Table 1. Time distributions of the comparison of annual values of physical quantities. The table lists values of Radiation Obs, the observed downward short-wave radiation ($\text{MJ m}^{-2}\text{day}^{-1}$), Cal, the calculated downward short-wave radiation ($\text{MJ m}^{-2}\text{day}^{-1}$), Sunshine Obs, the observed sunshine duration (hour day^{-1}), Soil Water, the soil water content (cm), Canopy Temp, the canopy temperature ($^{\circ}\text{C}$), and R. Humidity, the surface relative humidity (%). Precipitation is the precipitation (mm day^{-1}), L.H. Flux ET is the latent heat flux by transpiration ($\text{MJ m}^{-2}\text{day}^{-1}$), CO_2 Flux NET is the net carbon dioxide flux ($\text{mol m}^{-2}\text{day}^{-1}$), CO_2 Flux AAT is the total carbon dioxide assimilation flux ($\text{mol m}^{-2}\text{day}^{-1}$), and CO_2 Flux RES is the total respiration flux ($\text{mol m}^{-2}\text{day}^{-1}$). The canopy temperature and surface relative humidity are the 6-month mean values (May–October) for each year, while the others are annual means. The last column, R, lists the correlation coefficients between the net carbon dioxide flux and other quantities.

	1986	1987	1988	1989	1990	1991	R
Radiation							
Obs.	12.8	12.6	12.2	12.5	12.9	12.4	0.69
Cal.	9.9	10.1	9.4	9.5	9.9	9.1	0.92
Sunshine							
Obs.	5.4	5.0	4.3	4.4	4.5	4.1	0.87
Soil water	102.7	104.0	104.2	105.1	105.8	106.1	-0.67
Canopy temp.	15.8	16.4	15.9	15.9	16.9	16.6	-0.26
R. Humidity	91.9	91.9	92.5	92.4	92.9	92.9	-0.72
Precipitation							
	4.2	4.5	4.7	5.3	5.4	5.3	-0.55
L.H. Flux ET							
	1.6	1.6	1.3	1.5	1.6	1.3	0.88
CO_2 Flux NET	0.080	0.075	0.057	0.068	0.070	0.043	—
CO_2 Flux AAT	0.351	0.347	0.315	0.335	0.356	0.306	—
CO_2 Flux RES	0.271	0.272	0.258	0.267	0.286	0.263	—

The correlation coefficient between NET and the canopy temperature has a small negative value. This suggests that an adequate correlation does not exist between the canopy temperature and NET. From these discussions, it is suggested that the reason for the characteristic phenomenon of the stepwise increase in the lower tropospheric long-term trend in the CDC from 1987 to 1988 is as follows: interannual variations in the net carbon dioxide flux between the land surface ecosystems and the atmosphere influenced the lower tropospheric long-term trends of the CDC from 1986 through 1991 over the Japanese Islands. The characteristic interannual variations in the net carbon dioxide flux during that period were mainly controlled by interannual variations in the downward short-wave radiation at the land surface.

Studies using the physical climate model, including the biological scheme, are useful for understanding the physical and biological mechanisms in regional and global climate systems. Through the accurate reproduction of actual phenomena and with accurate interpretation, the mechanisms that produce such phenomena can be clarified in order to improve the estimates for future situations.

REFERENCES

- Kida, H., T. Koide, H. Sasaki and M. Chiba, 1991: A new approach for coupling a limited area model to a GCM for regional climate simulations. *J. Meteor. Soc. Japan*, **69**, 723–728.
- Mabuchi, K., Y. Sato, H. Kida, N. Saigusa and T. Oikawa, 1997: A Biosphere-Atmosphere Interaction Model (BAIM) and its primary verifications using grassland data. *Papers in Meteor. and Geophys.*, **47**, 115–140.
- Mabuchi, K., Y. Sato and H. Kida, 2000: Numerical study of the relationships between climate and the carbon dioxide cycle on a regional scale. *J. Meteor. Soc. Japan*, **78**, 25–46.
- Mabuchi, K., Y. Sato and H. Kida, 2001: Verification of the climatic features of a regional climate model with BAIM. *J. Meteor. Soc. Japan* (revising).
- Nakazawa, T., S. Morimoto, S. Aoki and M. Tanaka, 1993: Time and space variations of the carbon isotopic ratio of tropospheric carbon dioxide over Japan. *Tellus*, **45B**, 258–274.
- Tatsumi, Y., 1986: A spectral limited-area model with time-dependent lateral boundary conditions and its application to a multi-level primitive equation model. *J. Meteor. Soc. Japan*, **64**, 637–663.

K. Mabuchi (e-mail: kmabuchi@mri-jma.go.jp), Y. Sato and H. Kida